Optimized Interference Suppression for TCSPC LiDAR

Sara Grollius, Simon Grosse, Manuel Ligges, and Anton Grabmaier

***Abstract*—The increased use of light detection and ranging (LiDAR) systems for distance determination requires the investigation of mutual interference. In this article, we describe the conditions for the occurrence of LiDAR interference. We outline suppression methods for different LiDAR types identifying pulse-position modulation (PPM) as a solution for time-of-flight LiDAR with time-correlated single photon counting (TCSPC) histograms. Based on PPM, we present a suppression method, which randomly varies the laser pulse emission times. For optimal suppression, we switch on the suppression only when interference is present. To recognize the occurrence of LiDAR interference, we develop a multipulse detection algorithm that can also extract all pulse positions. Simulations show that the algorithm can be applied for a signal-to-noise ratio greater than 3. Determining the heights of all recognized pulse signatures, an appropriate suppression level can be chosen. We successfully show the optimized interference suppression for an example LiDAR measurement. For safe use by multiple systems, we suggest random numbers. We reuse the TCSPC histograms to generate random numbers, whose generation probability is calculated theoretically and confirmed by simulation and measurement data. For nearly all histogram distributions consisting of background- and laser-generated data, a sufficient amount of random numbers is produced.**

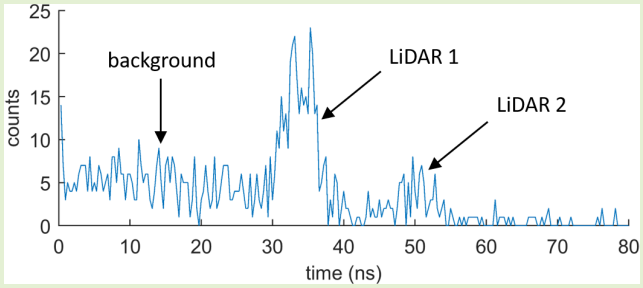

***Index Terms*—Mutual light detection and ranging (LiDAR) interference, pulse-position modulation (PPM), random number generation, time-correlated single photon counting (TCSPC), time-of-flight (TOF).**

I. Introduction

With increasing number of light detection and ranging (LiDAR) systems worldwide, the probability for mutual interference arises. Especially in uncontrolled environments as given in autonomous driving, two or more LiDAR systems can observe the same targets as shown in Fig. 1. Time-of-flight (TOF) LiDAR is a method to measure target distances by the emission of a laser pulse, which is reflected by a target back to the LiDAR sensor. The LiDAR system measures the TOF t_{TOF} of the laser pulse, which transforms into the target distance d by

$$d = \frac{c \cdot t_{\mathrm{TOF}}}{2} \tag{1}$$

where c is the speed of light [1]. Using a single-photon avalanche diode (SPAD) as a sensor, even single photons can be detected. After each detection, the SPAD becomes insensitive during a certain dead time. Therefore, usually, only the first photon is detected after the emission of each pulse. The arrival times of all first-photon detections are accumulated in a histogram as seen in Fig. 1. This method is called time-correlated single photon counting (TCSPC). Besides the laser pulse, constant background light might be detected, for example, from the sun. Since later photons are ignored, the first-photon principle overemphasizes earlier arrival times. The resulting count distribution in the histogram is exponentially distorted, which is known as the pile-up effect [2], [3], [4]. The expected histogram distribution with a single temporarily rectangular pulse can be described by the probability density function (PDF)

$$P(t) = \begin{cases} r_{\mathrm{B}} \mathrm{e}^{-r_{\mathrm{B}} t}, & 0 \leqslant t < t_{\mathrm{TOF}} \\ (r_{\mathrm{B}} + r_{\mathrm{L}})\, \mathrm{e}^{r_{\mathrm{L}} t_{\mathrm{TOF}}} \mathrm{e}^{-(r_{\mathrm{B}} + r_{\mathrm{L}}) t}, & t_{\mathrm{TOF}} \leqslant t < t_{\mathrm{TOF}} + t_{\mathrm{p}} \\ r_{\mathrm{B}} \mathrm{e}^{-r_{\mathrm{L}} t_{\mathrm{p}}} \mathrm{e}^{-r_{\mathrm{B}} t}, & t_{\mathrm{TOF}} + t_{\mathrm{p}} \leqslant t \end{cases} \tag{2}$$

where r_{B} and r_{L} are the background- and laser-generated event rates, respectively. t_{p} is the pulsewidth of the laser arriving at TOF t_{TOF}. In the case of LiDAR interference, laser pulses of other LiDAR systems can be seen in the histogram as shown in Fig. 1. These pulse signatures are generally indistinguishable so that the TOF of the own pulse and hence the target distance

Manuscript received 30 September 2022; accepted 10 October 2022. Date of publication 31 October 2022; date of current version 14 December 2022. The associate editor coordinating the review of this article and approving it for publication was Prof. Carlos Marques. *(Corresponding author: Sara Grollius.)*

Sara Grollius, Simon Grosse, and Manuel Ligges are with the Fraunhofer Institute for Microelectronics Circuits and Systems, 47057 Duisburg, Germany (e-mail: sara.grollius@ims.fraunhofer.de).

Anton Grabmaier is with the Department of Electronic Components and Circuits, University of Duisburg-Essen, 47057 Duisburg, Germany, and also with the Fraunhofer Institute for Microelectronic Circuits and Systems, 47057 Duisburg, Germany.

Digital Object Identifier 10.1109/JSEN.2022.3216810

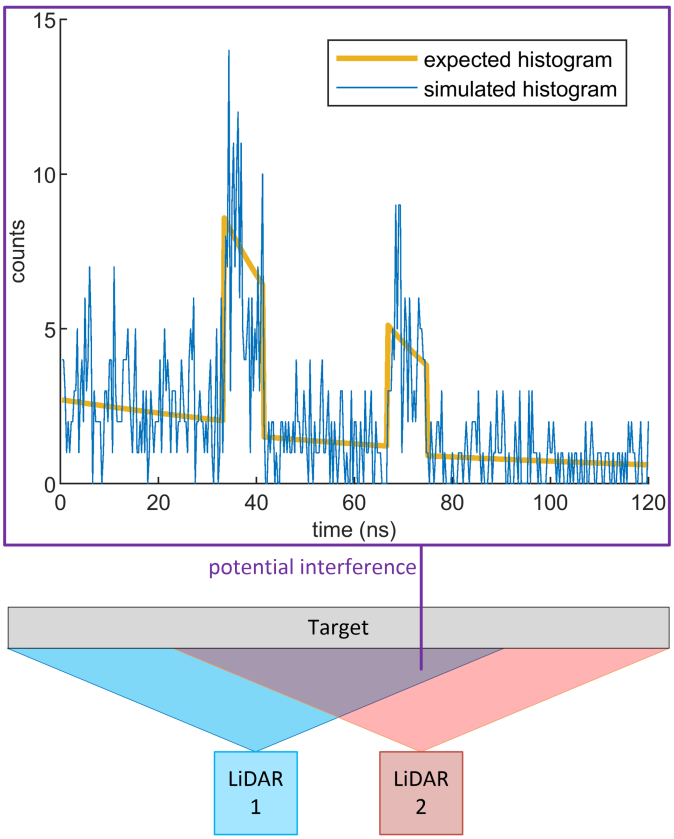

Fig. 1. Potential interference between two LiDAR systems can cause more than one laser pulse detection in the histogram.

cannot be clearly determined. The corresponding PDF for multiple pulse signatures in a histogram is given in [5]. In the following, we only consider detected pulse signatures from real objects of interest. In fact, additional pulse signatures in the histogram can be produced by weather conditions like rain or fog [6]. We neglect such contributions to the histogram for now, but the presented algorithms can be generally adopted for such cases.

In Section II, we introduce conditions for LiDAR interference. After that, we introduce related work on interference suppression. In Section V, we present a method to generate random numbers from TCSPC histograms, which is confirmed by simulation and measurement data from the LiDAR system OWL with sensor *CSPAD αlpha* developed at Fraunhofer IMS [7]. These random numbers are used for interference suppression described in Section IV. Finally, a conclusion is given.

II. Conditions for LiDAR Interference

Interference can only occur if the LiDAR systems use the same wavelength because their optical bandpass filters block all other wavelengths to reduce background light. Additionally, the LiDAR systems have to illuminate the same targets. For scanning systems, this happens comparatively rare when compared to flash systems because they frequently move their field-of-illumination (FOI), which is furthermore smaller than most flash illuminations. For interference, the interfering systems must perform their measurements at the same time. The measurement time is equivalent to the histogram length. For example, our used LiDAR system has a measurement time of 1.28 µs corresponding to 192 m according to (1). In contrast, the time between two emitted laser pulses is often higher because, after the measurement, the data must be read out and processed. Furthermore, lower laser pulse repetition frequencies allow for higher optical peak power considering the eye safety standard [8]. The used LiDAR system has a pulse repetition frequency (PRF) of 10 kHz referring to 100 µs between two pulses, which is much higher than the measurement time of 1.28 µs. When the LiDAR systems measure simultaneously, they can detect photons of the foreign laser pulse. However, not every interference disturbs the LiDAR measurement. For negative impacts, they must use exactly the same or multiples of the PRF so that repeated measurements of both systems continuously interfere and both laser pulse signatures accumulate in the histogram. Small deviations in the PRF, for example, by manufacturing tolerances can already distribute the foreign laser pulse in the histogram, whereas the own laser signal stays accumulated [5]. In this case, the strongly smeared signal width can be distinguished from the own laser pulse form. The accumulation of the own laser pulse signature in the histogram is unaffected by PRF changes because the measurement start is synchronized with the laser pulse emission. Assuming two LiDAR systems with equal PRFs and equal laser pulse widths, their pulse signatures in the histogram only differ by their heights and positions, which depends on the target's reflectance and distance. Therefore, it is unknown which signal in the histogram corresponds to the own emitted laser pulse.

III. Related Work

There are different LiDAR techniques, which are frequency-modulated continuous wave (FMCW), indirect time-of-flight (iTOF), and direct time-of-flight (dTOF) [9]. These techniques can be applied with different sensors, which can be divided into analog sensors like avalanche photodiodes (APDs) and digital sensors like SPADs. APDs are capable of measuring the real pulse forms, whereas SPADs measure skewed distributions due to the pile-up effect. The LiDAR systems can operate in controlled environments like industrial robots or in uncontrolled environments like autonomous driving. Controlled environments allow modification of the number of systems at the same location and the system properties as desired, whereas uncontrolled environments have an unknown number of LiDAR systems with unknown properties. For all different techniques, sensors, and environments, LiDAR interference behaves differently, and thus, different suppression methods are necessary.

There are different solutions known from the field of communication to avoid interference between multiple systems [10]. For controlled environments, space-division multiple access (SDMA) can be applied, where all systems have nonoverlapping field-of-views (FOVs). This is the best option if the systems are not moving but observe fixed spaces. Otherwise, if only a limited number of systems is present,

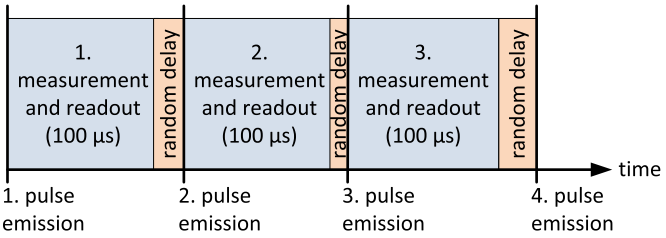

Fig. 2. Time diagram of PPM for a LiDAR system operating without suppression at a PRF of 10 kHz, which corresponds to 100 µs.

wavelength-division multiple access (WDMA) can be used, where every LiDAR system operates at a different wavelength with narrow optical bandpass filters. This method is limited by the wavelength range typically lying in the near-infrared spectrum, which is invisible to human eyes. Additionally, the sensor sensitivity depends on the wavelength, and certain wavelengths can be produced more easily. Silicon sensors are often used with 700–1000 nm [11], whereas more expensive InGaAs sensors are usually combined with 1550 nm [12], [13]. Overall, not many different wavelengths are available to differentiate LiDAR systems from each other. Similarly, amplitude-modulated continuous-wave (AMCW) LiDAR can apply CW lasers with different modulation frequencies, which is called frequency-division multiple access (FDMA). Here, the number of working implementations is limited as well with regard to the required measurement performance. For cooperative LiDAR systems, time-division MA (TDMA) is a good solution, where the systems are coordinated to perform alternating measurements. However, for uncontrolled environments with an unlimited number of LiDAR systems, the measurement times cannot be controlled and will probably overlap sometimes. In this case, only code-division MA (CDMA) is suitable, which encodes the light emitted by the LiDAR system. Usually, laser signals are emitted that are temporally modified. For example, the laser pulse form can be modulated [14] or coded pulse trains instead of single pulses are used [15], [16]. SPADs are not able to measure these temporal modulations within one measurement due to the first-photon principle causing the pile-up effect. Therefore, code-division multiple access (CDMA) with dual-pulse emission considering dead time [17], PPM [18], [19], [20], [21], [22], [23], or a combination of both methods is suggested [9], [10], [24].

IV. Interference Suppression

PPM is the temporal modulation of the pulse position so that the position of the own pulse signature in the histogram changes. Due to the known modulation pattern, the received photons can be correlated with the known emission pattern. The TOF is found by the position with the highest correlation. Alternatively, the measurement start can be modulated exactly like the laser pulse emission so that the received own pulse signature accumulates in the histogram as before. Instead, all foreign pulse signatures will change their positions in the histogram. We apply the second possibility in our LiDAR system. The corresponding time diagram for our LiDAR system is shown in Fig. 2. Without suppression, the operating PRF is 10 kHz corresponding to 100 µs between two consecutive pulses. The suggested suppression method inserts random delays before the laser pulse emissions. After each pulse emission, the measurement time of 1.28 µs is started, and the detected photon arrival time is read out.

Ideal LiDAR systems have lasers approaching the optical power limit of the eye safety standard [8]. Eye safety mainly affects the average optical power per time and space. Hence, PPM can only delay single pulses but not premature the laser emission, as this would violate the eye safety standard. Therefore, PPM reduces the frame rate. For example, autonomous driving requires a frame rate of 25 frames/s [25]. If the maximum delay of the emitted laser pulse is chosen equivalently to the total histogram length of 1.28 µs, the foreign laser pulse can be distributed over the total histogram representing a strong suppression. However, for such a large delay, the frame rate is decreased to 24.7 frames/s. This might be considered acceptable. For other applications like high-speed LiDAR, this frame rate loss can be critical. For example, a high-speed LiDAR system has a PRF of 1MHz, frame rate of 10 000 frames/s, and range up to 25 m corresponding to a histogram length of 170 ns [26]. PPM reduces the frame rate to 86% of the original one.

We suggest an optimal solution for interference suppression maintaining high frame rates. As described in section II, many conditions must be met to emerge interference. As optimum, suppression should only switch on if interference occurs. Therefore, we provide a new multipulse detection algorithm, which recognizes interference and moreover delivers information about every detected pulse signature in the histogram. This algorithm consists of the following steps:

1) pile-up correction;
2) background subtraction;
3) smoothing by moving average filter;
4) threshold to cut off fluctuations;
5) pulse condition: pulse signature width $\geq$3 bins.

First, the pile-up effect is corrected so that the original pulse shapes are regained with the event rates per bin produced at the LiDAR detector by the photon rates during a single laser pulse return [2], [3], [27]. Additionally, the detected exponential background distribution in the histogram becomes a uniform distribution again due to the pile-up correction. After that, this constant background distribution is subtracted. Now, the fluctuating count distribution is smoothed by a moving average filter, whose filter width is half of the original laser pulsewidth. The remaining fluctuations due to the background are cut off by a threshold at 3σ level of the background uncertainty, which increases exponentially due to the pile-up correction [3]. Finally, every pulse signature is identified that consists of minimum three connected bins. Each pulse signature maximum can be identified during a laser pulsewidth added to the determined rising edges of the pulse signature beginnings. Here, nonoverlapping pulses are assumed. For various background and laser-generated event rates, the algorithm is simulated ten times and averaged as shown in Fig. 3. An example of the simulated histograms is seen in Fig. 4(a). For this histogram, the result of the multipulse detection algorithm

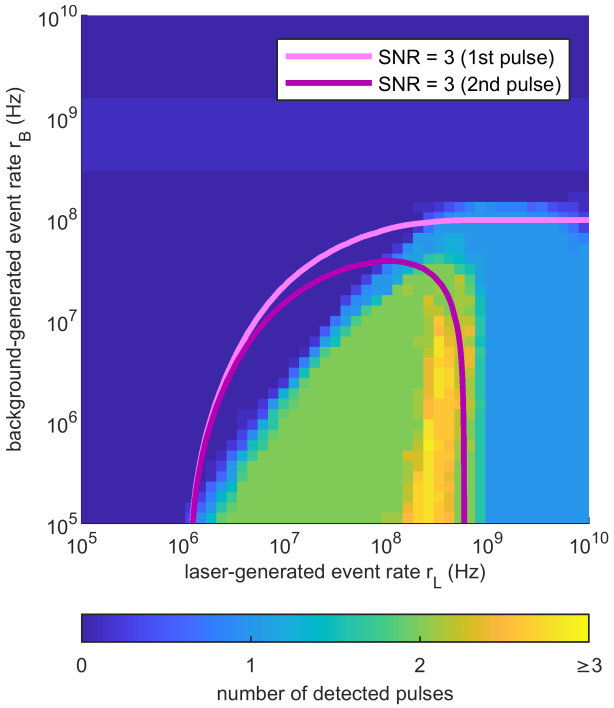

Fig. 3. Multipulse detection algorithm can approximately be applied for SNR $\geq$ 3.

is given in Fig. 4(b). In Fig. 3, the signal-to-noise ratio (SNR) value of the second lower pulse signature in the histogram is drawn by the equation given in [5]. In contrast to single pulse detections, the second pulse detection of interference is influenced by the first pulse signature in the histogram so that the signal-to-noise ratio (SNR) decreases again for high laser-generated event rates [5]. As seen, the algorithm can be applied for SNR values $\geq$3. Besides interference suppression, this algorithm is suitable for multiobject detection [28].

By the known pulse positions, the pulse signature heights in the original histogram can be identified. In the worst case, the own pulse signature is the lowest one. Therefore, interference suppression should provide the possibility to smear the highest pulse signature so much that it can fall below the lowest pulse signature height. Then, the highest pulse signature should correspond to the own laser pulse, whether it was the highest or lowest pulse signature in the previous histogram. In the presented histogram, the difference between the pulse signature heights is 3.5. Therefore, we choose a suppression level of 5, which is in the same order. In Fig. 4(c), we apply PPM as interference suppression with five different pulse positions in an arbitrary order based on random numbers. As result, the first pulse signature is distributed over the histogram and at its original position suppressed by a factor of about 3.5, whereas the second pulse signature remains the same. Obviously, the first pulse signature represents a disturbing interference signal from a foreign LiDAR system, whereas the second pulse signature represents its own laser pulse. Now, the required pulse position corresponding to the real target distance is determined. The presented method optimizes the interference suppression with regard to the frame rate.

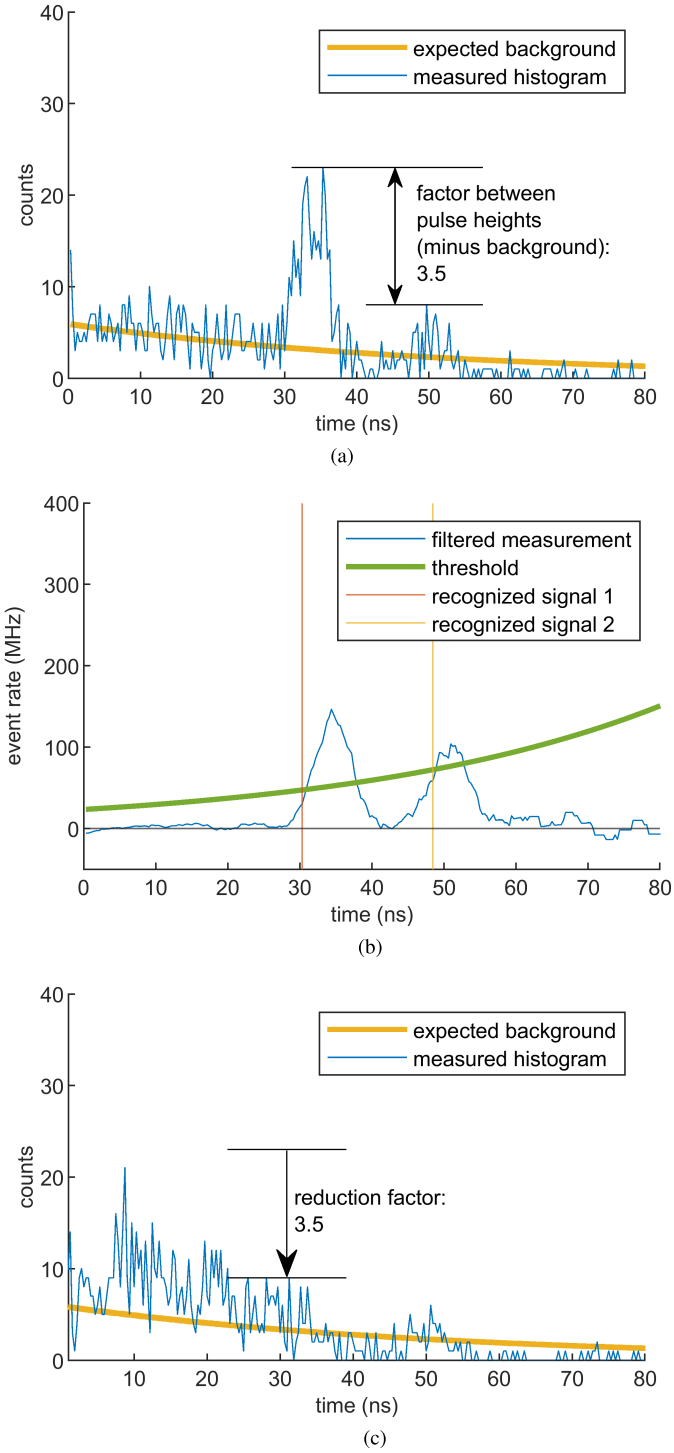

Fig. 4. Measurement with two pulse signatures in the histogram, which are both recognized. After that, optimal interference suppression is applied, which reduces the foreign pulse signature, whereas the own pulse signature remains. (a) Original histogram with the theoretically expected distribution. (b) Applied multipulse detection algorithm. (c) Histogram with optimized interference suppression.

For applications with uncritical frame rates, the previously described frame rate reduction might be acceptable so that PPM can be applied permanently with a high suppression level. In this case, the interference will not be recognized but immediately suppressed. However, the suppression level

must be strong enough to guarantee sufficient suppression for any possible scenario because a failed suppression will not be recognized. In contrast, the suggested method combining recognition and suppression provides the advantage that a low suppression level can be sufficient because the comparison of the histograms produced by the unsuppressed and suppressed measurements allows for easy identification of the right pulse signature.

V. Random Number Generation From TCSPC Histograms

PPM works well if the chosen pulse emission time pattern is only applied for a single LiDAR system, whereas all other systems still have regular pulse emissions. Applying PPM to many systems, it should be avoided that all systems use the same pattern synchronously because interference suppression is only achieved if the systems do not measure permanently at the same time. This is easily achieved if the different pulse emission times are modulated by random numbers. As a readily available random number source, we suggest the photon statistics given by TCSPC histograms, which are measured by digital sensors like the SPADs in our LiDAR system. Every single first-photon measurement delivers one arrival time, which is sorted in the histogram. To generate a random number, we compare pairs of two consecutive arrival times t_n and t_{n+1} for $n = 1, 3, 5, 7, \ldots$ to get the random number x as follows [29], [30]:

$$x = \begin{cases} 1, & t_n < t_{n+1} \\ 0, & t_n > t_{n+1} \\ /, & \text{else.} \end{cases} \tag{3}$$

If both arrival times have the same value $t_n = t_{n+1}$, no random number is received. The random number generation fails as well if one or both arrival times are nondetections, which means that no photon arrives during the measurement time. Therefore, ideal histograms should have a uniform distribution over all bins. Due to the pile-up effect, the number of early-arriving photons with equal arrival times can be increased so that no random numbers can be generated. However, the order of early or late-arriving photons is not influenced by the pile-up effect but is completely random. Considering the pile-up effect, an approximately uniform histogram distribution is achieved for low intensities, where the exponential distribution in the histogram becomes nearly constant so that the probability for equal photon arrival times is low. At the same time, the illumination intensity should be high enough to avoid nondetections. The generated random numbers provide a very low probability of two LiDAR systems generating the same random sequences because of the physical randomness of the photons [31]. In comparison, pseudorandom number generators might be easier to attack [32]. Additionally, the suggested random number generator can be easily implemented on a software level. Alternatively, a potential hardware implementation would only consist of a comparator for the arrival time comparison, which is also easy to be implemented.

In this article, we use typical LiDAR scenarios as an illumination source and evaluate their ability to generate random numbers. LiDAR histograms can contain either only background photon detections, primary the laser pulse photon detections or a combination of background and laser photon detections as seen in Fig. 1. The histograms have bin width 312.5 ps and 4096 bins corresponding to 192 m after (1). The pulse has a width of 8 ns and is set to a histogram position equivalent to 1 m.

TABLE I
Parameters of Theory, Simulation, and Measurement

Parameter	Symbol	Value
background-generated event rate	r_B	10^5 Hz -10^{10} Hz
laser-generated event rate	r_L	10^5 Hz -10^{10} Hz
pulse width	t_p	8 ns
bin width	t_bin	312.5 ps
histogram length	t_hist	1.28 µs
time-of-flight (TOF)	t_TOF	0 µs − 1.28 µs
signal-to-noise ratio (SNR)	−	3

To evaluate the yield of random numbers for all possible LiDAR scenarios, we have calculated the probability to generate random numbers. Based on the PDF $P(t)$ in (2), the probability p_miss that the first or the second or both arrival times are missing due to nondetection is given by

$$p_\mathrm{miss} = 2 \cdot p_\mathrm{non} - p_\mathrm{non}^2 \tag{4}$$

where p_non is the probability for a single nondetection given by

$$p_\mathrm{non} = 1 - \int_0^{t_\mathrm{hist}} P(\tau)\,\mathrm{d}\tau = \mathrm{e}^{-r_\mathrm{L} t_\mathrm{p}} \mathrm{e}^{-r_\mathrm{B} t_\mathrm{hist}} \tag{5}$$

where t_hist is the histogram length. The probability p_equal for two equal arrival times depends on the probability p_i to detect a photon in bin i. Considering all bins $i = 1, \ldots, n_\mathrm{bin}$, this probability is given by

$$p_\mathrm{equal} = \sum_{i=1}^{n_\mathrm{bin}} p_i^2. \tag{6}$$

The required bin probability p_i must be evaluated for all histogram parts by

$$p_i = \int_t^{t+t_\mathrm{bin}} P(\tau)\,\mathrm{d}\tau \tag{7}$$

where t_bin is the bin width, which is 312.5 ps for our LiDAR system. The probability for two valid arrival times generating a random number is derived by the probability of the first arrival time within bin i and the second arrival time excluding nondetection or again bin i given by

$$p_\mathrm{valid} = p_i \cdot (1 - p_\mathrm{non} - p_i). \tag{8}$$

The results of these probabilities are presented in Fig. 5. For pure background histograms, the theoretical probabilities are calculated and compared to simulation data. Each simulation result is averaged by ten simulations with a pulsewidth of 8 ns and a single target at 1 m. Additionally, measurement data are generated by our LiDAR system OWL with sensor *CSPAD alpha* [7]. The parameters for theory, simulation, and measurement are summarized in Table I. The resulting

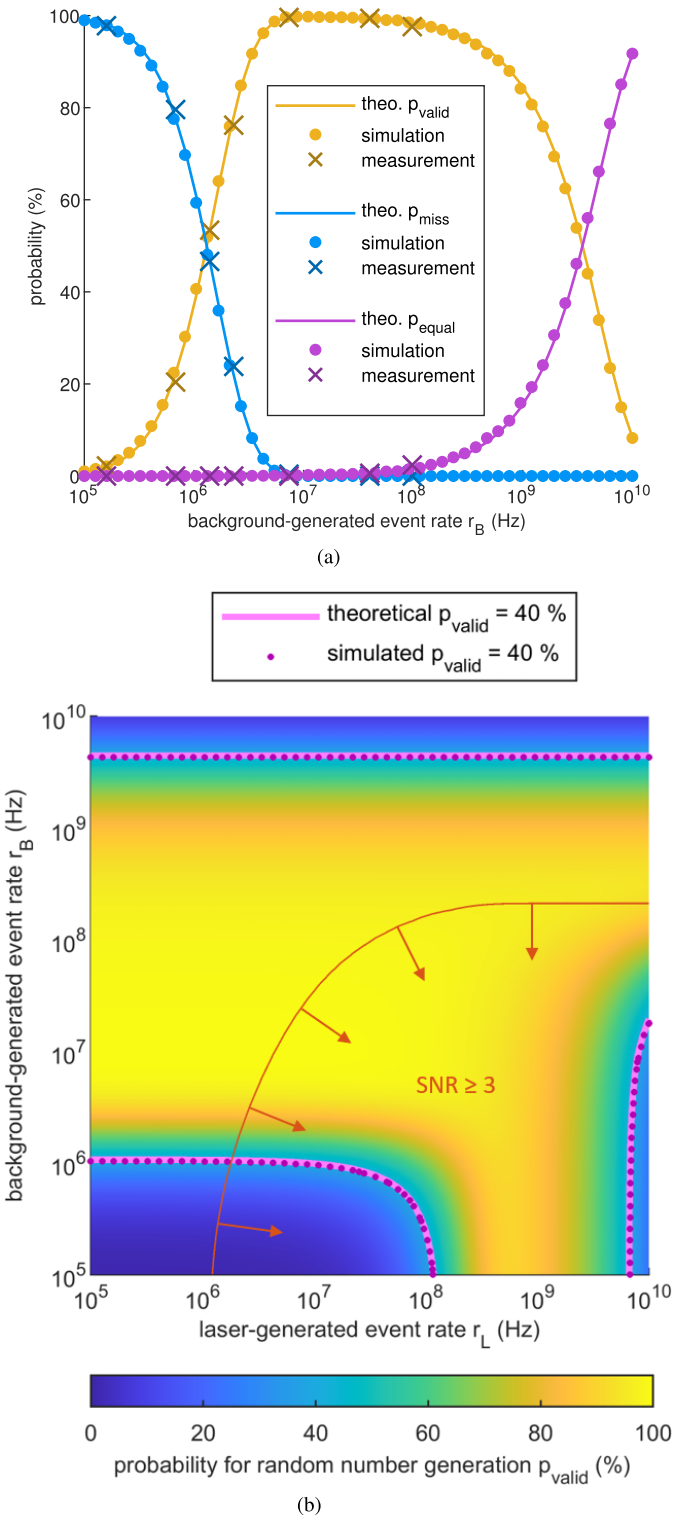

Fig. 5. Probability for random number generation by TCSPC histograms (with single pulse signature). The theoretical derivation is confirmed by simulation and measurement data. (a) Probability for successful random number generation by two valid time stamps and for an invalid time stamp pair due to missing detections or equal time stamps. (b) Probability for all possible event rates of background (r_B) and laser (r_L). Simulation and measurement data are illustrated by the arbitrarily chosen contour line of $p_{valid} = 40\%$. Histograms with evaluable laser pulse position are shown for SNR ≥ 3 below the orange contour line.

probabilities are shown in Fig. 5(a). The theory matches very well with simulation and measurement. The calculated probabilities p_{valid} are determined for every possible combination of background-generated event rate r_B and a single pulse signature with laser-generated event rate r_L as illustrated in Fig. 5(b). These event rates produced at the LiDAR detector are proportional to the photon rates of the arriving laser and background photons. The orange contour line illustrates the SNR at value 3 calculated in the histogram by the SNR equation in [5]. The SNR provides an impression, which histograms might be evaluable with regard to target distance determination by an appropriate algorithm [33]. Above this line, the pulse signature is hard to be recognized in the histogram but random number generation still works very well. The generation probability p_{valid} becomes zero at the bottom left corner because too few photons arrive so that many nondetections occur. In the top area, the high background results in a steep exponential distribution falling to zero within a few bins. The high counts within a few bins lead to many equal time stamps preventing random number generation. The bottom right corner shows the same effect for the laser distribution. The difference between background and laser is that the laser has a narrow width, which is rather disadvantageous with regard to random number generation. Additionally, the high laser pulse signature reduces the background distribution afterward due to first-photon detection. This is seen for the background-generated event rate $r_B = 10^7$ Hz, which works quite well for low laser-generated event rates but becomes critical for $r_L = 10^{10}$ Hz. To compare again with simulations, an arbitrary contour line at probability $p_{valid} = 40\%$ is drawn. Again, the simulation confirms the theory very well.

PPM does not require many random numbers. For nonoverlapping foreign pulse signatures in the histogram, the emission time of the own laser pulse should be delayed by a minimum of one pulsewidth, which is 8 ns for our interfering laser. If we move this foreign pulse signature over our total histogram with a length of 1.28 µs, there are 160 possible pulse signature positions in the histogram. Therefore, 1 byte of random numbers with $2^8 - 1 = 255$ possible positions is sufficient. In our case, the number of accumulated measurements per histogram is $n_{meas} = 1000$. Thus, we need 1000 bytes of random numbers from the last histogram to start the next acquisition. In the best case, a single histogram with 1000 arrival times delivers 500 random bits with values 0 or 1. Assuming this maximum yield, only 16 pixels are required to obtain $16 \cdot 500 = 8000$ bits $= 1000$ bytes. Considering the number of total pixels $32 \times 24 = 768$ of our LiDAR system, only $p_{valid} = 2\%$ of random number generation must be successful. As seen in Fig. 5(b), the required probability for random number generation $p_{valid} \geq 2\%$ is greatly exceeded for almost all event rates. Thus, there is no significant influence of the external illumination on the required random number generation for PPM.

VI. Conclusion

The increased use of LiDAR systems makes mutual LiDAR interference a relevant topic to be discussed. In this work, we summarize conditions for disturbing LiDAR interference due to identical LiDAR systems measuring simultaneously. We present related work with suppression methods for dif-

ferent LiDAR types. Focusing on dTOF LiDAR with TCSPC histograms measured by digital sensors like SPADs, only PPM appears suitable as interference suppression. PPM modulates the pulse emission times by a defined pattern. We suggest an optimized suppression method based on PPM using random numbers, which is switched on only when necessary. For this purpose, we develop a multipulse detection algorithm, which is capable of interference recognition and multiobject detection as well. The determined pulse signature heights allow for optimized interference suppression with a suppression level sufficient for the highest pulse signature. Applying our method, successful recognition of the own pulse signature is achieved. For the pulse emission time pattern, we extract random numbers from TCSPC histograms so that this method can be easily and safely used by multiple systems at the same time. As an outlook, this interference suppression method using random numbers instead of fixed patterns can be implemented in multiple LiDAR systems. This allows us to analyze the potential of random numbers to improve the probability that the systems measure asynchronously.

REFERENCES

[1] P. Seitz and A. J. Theuwissen, *Single-Photon Imaging*. Berlin, Germany: Springer, 2011.

[2] P. B. Coates, "The correction for photon 'pile-up' in the measurement of radiative lifetimes," *J. Phys. E, Sci. Instrum.*, vol. 1, no. 8, pp. 878–879, Aug. 1968.

[3] A. Gupta, A. Ingle, A. Velten, and M. Gupta, "Photon-flooded single-photon 3D cameras," in *Proc. IEEE/CVF Conf. Comput. Vis. Pattern Recognit. (CVPR)*, Jun. 2019, pp. 6763–6772.

[4] K. Pasquinelli, R. Lussana, S. Tisa, F. Villa, and F. Zappa, "Single-photon detectors modeling and selection criteria for high-background LiDAR," *IEEE Sensors J.*, vol. 20, no. 13, pp. 7021–7032, Jul. 2020.

[5] S. Grollius, A. Buchner, M. Ligges, and A. Grabmaier, "Probability of unrecognized LiDAR interference for TCSPC LiDAR," *IEEE Sensors J.*, vol. 22, no. 13, pp. 12976–12986, Jul. 2022.

[6] S.-Y. Tsai, Y.-C. Chang, and T.-H. Sang, "SPAD LiDARs: Modeling and algorithms," in *Proc. 14th IEEE Int. Conf. Solid-State Integr. Circuit Technol. (ICSICT)*, Oct. 2018, pp. 1–4.

[7] J. F. Haase, S. Grollius, S. Grosse, A. Buchner, and M. Ligges, "A 32×24 pixel SPAD detector system for LiDAR and quantum imaging," in *Proc. SPIE*, vol. 11693, Mar. 2021, Art. no. 116930M.

[8] *Safety of laser products*, IEC Standard 60 825-1, 2014.

[9] F. Villa, F. Severini, F. Madonini, and F. Zappa, "SPADs and SiPMs arrays for long-range high-speed light detection and ranging (LiDAR)," *Sensors*, vol. 21, no. 11, p. 3839, Jun. 2021.

[10] B. Buttgen and P. Seitz, "Robust optical time-of-flight range imaging based on smart pixel structures," *IEEE Trans. Circuits Syst. I, Reg. Papers*, vol. 55, no. 6, pp. 1512–1525, Jun. 2008.

[11] O. Skorka and D. Joseph, "CMOS digital pixel sensors: Technology and applications," in *Proc. SPIE*, vol. 9060, Apr. 2014, Art. no. 90600G.

[12] Y. Li and J. Ibanez-Guzman, "Lidar for autonomous driving: The principles, challenges, and trends for automotive lidar and perception systems," *IEEE Signal Process. Mag.*, vol. 37, no. 4, pp. 50–61, Jul. 2020.

[13] C. Bradley, S. Mukherjee, A. Reinhardt, P. F. Mcmanamon, A. Lee, and V. Dhulla, "3D imaging with 128×128 eye safe InGaAs p-i-n lidar camera," in *Proc. SPIE*, vol. 11005, pp. 273–279, May 2019.

[14] I. Hwang and C. Lee, "Mutual interferences of a true-random LiDAR with other LiDAR signals," *IEEE Access*, vol. 8, pp. 124123–124133, 2020.

[15] B. Büttgen, M.-A. E. Mechat, F. Lustenberger, and P. Seitz, "Pseudonoise optical modulation for real-time 3-D imaging with minimum interference," *IEEE Trans. Circuits Syst. I, Reg. Papers*, vol. 54, no. 10, pp. 2109–2119, Oct. 2007.

[16] T. Fersch, R. Weigel, and A. Koelpin, "A CDMA modulation technique for automotive time-of-flight LiDAR systems," *IEEE Sensors J.*, vol. 17, no. 11, pp. 3507–3516, Mar. 2017.

[17] H. Seo et al., "Direct TOF scanning LiDAR sensor with two-step multievent histogramming TDC and embedded interference filter," *IEEE J. Solid-State Circuits*, vol. 56, no. 4, pp. 1022–1035, Apr. 2021.

[18] D. U. Fluckiger, B. F. Boland, and E. Marcus, "Optimal pseudorandom pulse position modulation ladar waveforms," *Appl. Opt.*, vol. 54, no. 9, pp. 2183–2186, Mar. 2015.

[19] L. Carrara and A. Fiergolski, "An optical interference suppression scheme for TCSPC flash LiDAR imagers," *Appl. Sci.*, vol. 9, no. 11, p. 2206, May 2019.

[20] A. R. Ximenes, P. Padmanabhan, M.-J. Lee, Y. Yamashita, D.-N. Yaung, and E. Charbon, "A modular, direct time-of-flight depth sensor in 45/65-nm 3-D-stacked CMOS technology," *IEEE J. Solid-State Circuits*, vol. 54, no. 11, pp. 3203–3214, Nov. 2019.

[21] P. Du, F. Zhang, Z. Li, Q. Liu, M. Gong, and X. Fu, "Single-photon detection approach for autonomous vehicles sensing," *IEEE Trans. Veh. Technol.*, vol. 69, no. 6, pp. 6067–6078, Jun. 2020.

[22] T.-H. Sang, N.-K. Yang, Y.-C. Liu, and C.-M. Tsai, "A method for fast acquisition of photon counts for SPAD LiDAR," *IEEE Sensors Lett.*, vol. 5, no. 3, pp. 1–4, Mar. 2021.

[23] Y. Yu et al., "Detection probability analysis of true random coding photon counting LiDAR," *Photonics*, vol. 8, no. 12, p. 545, Nov. 2021.

[24] G. Kim and Y. Park, "Suitable combination of direct intensity modulation and spreading sequence for LIDAR with pulse coding," *Sensors*, vol. 18, no. 12, p. 4201, Nov. 2018.

[25] I. Maksymova, C. Steger, and N. Druml, "Review of LiDAR sensor data acquisition and compression for automotive applications," *Multidisciplinary Digit. Publishing Inst. Proc.*, vol. 2, pp. 852–855, Dec. 2018.

[26] J. Nissinen and J. Kostamovaara, "A high repetition rate CMOS driver for high-energy sub-ns laser pulse generation in SPAD-based time-of-flight range finding," *IEEE Sensors J.*, vol. 16, no. 6, pp. 1628–1633, Mar. 2016.

[27] A. K. Pediredla, A. C. Sankaranarayanan, M. Buttafava, A. Tosi, and A. Veeraraghavan, "Signal processing based pile-up compensation for gated single-photon avalanche diodes," 2018, *arXiv:1806.07437*.

[28] J. F. Haase, M. Beer, J. Ruskowski, and H. Vogt, "Multi object detection in direct time-of-flight measurements with SPADs," in *Proc. 14th Conf. Ph.D. Res. Microelectron. Electron. (PRIME)*, Jul. 2018, pp. 237–239.

[29] D. Thiem, "Entwicklung eines quantum random number generators (QRNG) basierend auf der CSPAD technologie," B.S. thesis, Inst. Natural Sci., Ruhr West Univ. Appl. Sci., Mülheim, Germany, Feb. 2020.

[30] A. Stanco, D. G. Marangon, G. Vallone, S. Burri, E. Charbon, and P. Villoresi, "Efficient random number generation techniques for CMOS single-photon avalanche diode array exploiting fast time tagging units," *Phys. Rev. Res.*, vol. 2, no. 2, Jun. 2020, Art. no. 023287.

[31] B. Liu, Y. Yu, Z. Chen, and W. Han, "True random coded photon counting LiDAR," *Opto-Electron. Adv.*, vol. 3, no. 2, Feb. 2020, Art. no. 190044.

[32] J. Melià-Seguí, J. Garcia-Alfaro, and J. Herrera-Joancomartí, "A practical implementation attack on weak pseudorandom number generator designs for EPC Gen2 tags," *Wireless Pers. Commun.*, vol. 59, no. 1, pp. 27–42, Jul. 2011.

[33] A. Buchner et al., "Analytical evaluation of signal-to-noise ratios for avalanche- and single-photon avalanche diodes," *Sensors*, vol. 21, no. 8, p. 2887, Apr. 2021.

Sara Grollius received the bachelor's and M.Sc. degrees in physics from the University of Wuppertal, Wuppertal, Germany, in 2015 and 2018, respectively. She is currently pursuing the Ph.D. degree in electrical engineering with the Fraunhofer Institute for Microelectronic Circuits and Systems (IMS), Duisburg, Germany.

Her topic is the quality and reliability of light detection and ranging (LiDAR) systems, which determine target distances by the principle of direct time-of-flight.

Simon Grosse received the bachelor's and M.Sc. degrees in nanoengineering with a specialization in nanooptoelectronics from the University of Duisburg-Essen, Duisburg, Germany, in 2014 and 2017, respectively.

He is a Research Assistant at the Fraunhofer Institute for Microelectronic Circuits and Systems, Duisburg, Germany. His research interests include SPAD-based sensors, optical systems, and applications of single-photon detection.

Manuel Ligges received the Diploma and Ph.D. degrees in physics from the University of Duisburg-Essen, Duisburg, Germany, in 2005 and 2009, respectively.

Until 2019, he worked as a Research Assistant and an Assistant Professor in the field of solid-state physics. He leads the Group of Optical Systems, Fraunhofer Institute for Microelectronic Circuits and Systems (IMS), Duisburg.

Anton Grabmaier received the Diploma and Ph.D. degrees in physics specializing in semiconductor physics and measurement technology from the University of Stuttgart, Stuttgart, Germany, in 1983 and 1989, respectively. His dissertation was focused on laser diodes.

Since 2006, he has been a Professor at the University of Duisburg-Essen, Duisburg, Germany. He is working as the Director of the Fraunhofer Institute for Microelectronic Circuits and Systems (IMS), Duisburg, Germany.